Biochimica et Biophysica Acta 1788 (2009) 1081–1091

Contents lists available at ScienceDirect

Biochimica et Biophysica Acta

journal homepage: www.elsevier.com/locate/bbamem

ATP and magnesium drive conformational changes of the Na^+/K^+-ATPase cytoplasmic headpiece

Lenka Grycova [a], Petr Sklenovsky [b], Zdenek Lansky [a], Marika Janovska [c], Michal Otyepka [b], Evzen Amler [d], Jan Teisinger [a], Martin Kubala [c,*]

[a] Institute of Physiology, Academy of Sciences of the Czech Republic, Vídeňská 1083, 14220 Prague 4, Czech Republic
[b] Department of Physical Chemistry, Faculty of Sciences, Palacký University in Olomouc, tř. Svobody 26, 77146 Olomouc, Czech Republic
[c] Laboratory of Biophysics, Faculty of Sciences, Palacký University in Olomouc, tř. Svobody 26, 77146 Olomouc, Czech Republic
[d] Institute of Biophysics, Second Faculty of Medicine, Charles University in Prague, Czech Republic

ARTICLE INFO

Article history:
Received 24 September 2008
Received in revised form 16 January 2009
Accepted 3 February 2009
Available online 20 February 2009

Keywords:
Na^+/K^+-ATPase
P-type ATPase
ATP
Magnesium
Tryptophan fluorescence
Conformational change

ABSTRACT

Conformational changes of the Na^+/K^+-ATPase isolated large cytoplasmic segment connecting transmembrane helices M4 and M5 (C45) induced by the interaction with enzyme ligands (i.e. Mg^{2+} and/or ATP) were investigated by means of the intrinsic tryptophan fluorescence measurement and molecular dynamic simulations. Our data revealed that this model system consisting of only two domains retained the ability to adopt open or closed conformation, i.e. behavior, which is expected from the crystal structures of relative Ca^{2+}-ATPase from sarco(endo)plasmic reticulum for the corresponding part of the entire enzyme. Our data revealed that the C45 is found in the closed conformation in the absence of any ligand, in the presence of Mg^{2+} only, or in the simultaneous presence of Mg^{2+} and ATP. Binding of the ATP alone (i.e. in the absence of Mg^{2+}) induced open conformation of the C45. The fact that the transmembrane part of the enzyme was absent in our experiments suggested that the observed conformational changes are consequences only of the interaction with ATP or Mg^{2+} and may not be related to the transported cations binding/release, as generally believed. Our data are consistent with the model, where ATP binding to the low-affinity site induces conformational change of the cytoplasmic part of the enzyme, traditionally attributed to E2 → E1 transition, and subsequent Mg^{2+} binding to the enzyme–ATP complex induces in turn conformational change traditionally attributed to E1 → E2 transition.

1. Introduction

The Na^+/K^+-ATPase (sodium pump, EC 3.6.3.9) translocates sodium and potassium ions across the plasma membrane against their concentration gradients using the energy from ATP hydrolysis. This is crucial for maintaining both the membrane potential and low cytoplasmic sodium concentration. As the gradient of sodium is also used by several secondary transporters of various solutes, it is not surprising that malfunction of the Na^+/K^+-ATPase is involved in pathology of several dozens of diseases, like e.g. ischemia or diabetes.

Na^+/K^+-ATPase belongs to the P-type ATPases superfamily [1]. Its designation is derived from the finding that the enzyme is autophosphorylated during the catalytic cycle. The Albers–Post model postulates that the enzyme adopts two conformations during the catalytic cycle, which are traditionally designated as E1 and E2 [2,3]. The enzyme in the E1 conformation has a high affinity to both ATP and sodium ions, while in the E2 conformation it has a low affinity to ATP and a high affinity to potassium. The cations binding sites, which are located within the transmembrane domain, are open toward cytoplasm in the E1 conformation and toward extracellular milieu in the E2 conformation. Notably, already early experiment of Skou [4] revealed the important role of the Mg^{2+} cations for the proper function of the enzyme. Although Mg^{2+} is not transported across the plasma membrane, it must be present in the cytoplasm as an essential cofactor.

Na^+/K^+-ATPase and H^+/K^+-ATPase are the only members of the P-type ATPases superfamily characterized by the presence of two subunits. The catalytic α-subunit contains the conserved sequences characteristic for the P-type ATPase superfamily [5] and it is responsible for the cations translocation as well as ATP hydrolysis. The β-subunit is a glycoprotein with single transmembrane helix and it is essential for the proper maturation and targeting of the enzyme

Abbreviations: Na^+/K^+-ATPase, sodium pump; SERCA, sarco(endo)plasmic reticulum; M1–M10, ten transmembrane helices; C23, cytoplasmic segment connecting the second and third transmembrane helices, other cytoplasmic segments analogously; TNP-ATP, [2′,3′-O-(2,4,6-trinitrophenyl)adenosine 5′-triphosphate; PCR, polymerase chain reaction; IPTG, isopropyl β-D-thiogalactoside; PMSF, Phenylmethylsulfonyl fluoride; DTT, dithiothreitol; SDS, PAGE, sodium dodecyl sulfate polyacrylamide gel electrophoresis; MD, molecular dynamics; PME, the particle-mesh Ewald; RMSD, root-mean-square-deviation; R_g, radius of gyration; RDF, radial distribution function; $^{O/C}E_{Na/K}$, superscipts O and C means open/close conformation and subscript represent high affinity of the sodium and potasium ions to the transmembrane domain; CH, cytoplasmic headpiece; TD, transmembrane domain

* Corresponding author.
E-mail address: mkubala@prfnw.upol.cz (M. Kubala).

0005-2736/$ – see front matter © 2009 Elsevier B.V. All rights reserved.
doi:10.1016/j.bbamem.2009.02.004

into the plasma membrane, though it is very likely that it interacts with the α-subunit also during the catalytic cycle [6].

Successful crystallization of another P-type ATPase family member, the Ca^{2+}-ATPase from sarco(endo)plasmic reticulum (SERCA, EC 3.6.3.8), provided a very valuable information about the structure of the catalytic subunit [7]. Moreover, SERCA was later crystallized in various conformations that were assigned to the E1 or E2 states of the enzyme [8–16]. There are numerous spectroscopic and biochemical experiments suggesting that the topologies of the Na^+/K^+-ATPase α-subunit and SERCA are very similar [for review, see [17]]. They were recently supported by the publication of the Na^+/K^+-ATPase crystal structure at 3.5 Å resolution [18], which confirmed the close structural relationship of these two enzymes. The α-subunit has ten transmembrane helices (M1–M10) and two longer cytoplasmic segments that are organized into three well-separated domains. The one, designated as A, is formed by the C23 (cytoplasmic segment between the M2 and M3), the other two, designated as N and P are formed by C45. Designation of the P-domain has origin in the fact that it contains the phosphorylated aspartyl residue, the N-domain contains the nucleotide-binding site and the A-domain (actuator or anchor) assists to the conformational changes that are necessary for the cation transport. The cation-binding sites are located within the transmembrane region; the cations are coordinated by the residues of M4, M5, M6 and M8 [7].

It was shown that the large cytoplasmic segment C45 of the α-subunit containing both the nucleotide binding- and phosphorylation sites can be overexpressed in *E. coli* and purified without the rest of the enzyme [19–23]. It was demonstrated that this isolated C45 retains its functional properties, such as ATP- or TNP-ATP-binding, suggesting that the 3D-structure is preserved [19–25]. This is also supported by the finding that the structure of the isolated N-domain independently solved by both NMR and crystallography fitted well to the N-domain from the crystals of SERCA [26]. This artificial system became popular, because (i) it uncouples the enzyme/nucleotide interaction from the cation transport, which facilitates the data interpretation, and (ii) solubility of the isolated C45 greatly facilitates the experimental work.

Intrinsic tryptophan fluorescence is very sensitive to the changes in the environment of the tryptophanyl residue, and thus, it could be a useful marker of the conformational changes. However, in order to localize the molecular events, the spectroscopic data can be easily interpreted only for a protein that contains no more than a single Trp residue. Therefore, we have created a set of single-tryptophan mutants of the C45, and monitored changes induced on the C45 upon interaction with the Mg^{2+}, Na_2ATP or MgATP ligands. Our data indicate that ATP and magnesium act in a coordinated manner in order to open or close the C45. As the abovementioned crystallographic studies provide only the static structural information, our experiments monitoring the C45 dynamic well complement these data.

2. Materials and methods

2.1. Site-directed mutagenesis of the Na^+/K^+-ATPase C45

DNA sequence of the C45 of the Na^+/K^+-ATPase α-subunit was prepared by the polymerase chain reaction (PCR) from the 1260 base DNA segment encoding Lys354–Lys774 α1-subunit of the mouse brain Na^+/K^+-ATPase used previously in our laboratory [21–23,27]. This sequence (L354 – I777) was amplified using the primers allowing the introduction of NheI and HindIII restriction sites at the 5′ and 3′ termini, double digested with NheI, HindIII restriction enzymes, and ligated into the expression vector pET28b. DNA sequencing of the resulting construct was performed on ABI Prism automated sequencer (facility of the Academy of Sciences of the Czech Republic) in order to confirm the in-frame insertion of the C45 DNA into the expression vector. The wild-type sequence of the C45 contains two native tryptophan residues W411 and W385. These two amino acid residues were subsequently substituted by phenylalanine residues, yielding two single-tryptophan mutants WT-W385F and WT-W411F and the tryptophanless (TL) double mutant WT-W411F-W385F, which was thereafter used as a template for other point mutations. Following single-tryptophan mutants were constructed: TL-F404W, TL-F426W, TL-F571W, TL-I627W, TL-F683W, and TL-S732W. Site directed mutagenesis PCRs were performed using PfuUltra High-fidelity DNA Polymerase (Stratagene). The upstream primers for performed mutations were (altered nucleotides are in italic):

WT-W385F 5′ggatgacagtggctcacatg*ttc*tttgacaatcaaatcc3′,
TL-F404W 5′gagaatcagagtggggtctcctgggacaagacgtcagccacc3′,
WT-W411F 5′gacaagacgtcagccacc*ttc*ttcgctctgtccagaattgc3′,
TL-F426W 5′tgtaacagggcagtgtggcaggctaaccaagaaaacc3′,
TL-F571W 5′gacactgatgaagtcaattggcccgtggataacctctgc3′,
TL-I627W 5′gggggtgggcat*ttg*gtcagaaggtaacg3′,
TL-F683W 5′gcggtaccacacggagattgtctgggctaggacctctcctc3′,
TL-S732W 5′gccatggggattgttggctgggatgtgtccaagc3′.

Downstream primers were reverse complementary. All constructs were verified by DNA sequencing.

2.2. Fusion protein expression and purification

The C45 of the Na^+/K^+-ATPase DNA and all its mutations were transformed into BL21 *Escherichia coli* bacteria (Promega) and were cultured at 37 °C to OD(600 nm) of 0.6. Induction was carried out with 0.2 mM IPTG (isopropyl β-D-thiogalactoside) overnight at 17 °C. Cells were centrifuged, resuspended in 20 mM Tris–HCl, 140 mM NaCl, pH 7.4 containing protein inhibitors (2 μg/ml leupeptin, 2 μg/ml pepstatin and 1 mM Phenylmethylsulfonyl fluoride (PMSF)), disrupted by sonication and the homogenate was again centrifuged. All constructs were expressed as a $(His)_6$ – tag fusion protein; the $(His)_6$ – tag was attached to the N-terminus. Purification affinity chromatography was performed according to standard TALON Metal Affinity Resin (Clontech) manufacturer protocol. The protein samples were eluted with 0.5 M Imidazol and were dialyzed against 1 liter of 50 mM Tris–HCl, 140 mM NaCl, 2 mM DTT, pH 7.5 overnight at 4 °C. The purity of protein samples was verified using 12% SDS-PAGE. Concentrations were estimated using the Bradford assay [28].

2.3. Tryptophan fluorescence quenching

The steady-state tryptophan fluorescence emission was quenched using 0–300 mM acrylamide as a quencher. Data were collected using an excitation and emission wavelengths of 295 nm and 360 nm, respectively, slits were set to 5 nm and 10 nm for the excitation and emission channel, respectively, the integration time was 3 s for recording of each point, the measurements were performed at 22 °C. Protein samples were diluted to the final 3 μM concentration into 20 mM Tris–HCl, 140 mM NaCl, pH 7.5 buffer, where oxygen was removed by argon, and were titrated by aliquots of the quencher. The sample was gently stirred and the fluorescence spectrum was recorded.

The efficiency of quenching was evaluated by the non-linear least-squares analysis using the Stern–Volmer formula:

$$F = \frac{F_0}{1 + K_{SV}[Q]}$$

where F_0 and F are the fluorescence intensities in the absence or in the presence of the quencher, respectively, K_{SV} is the Stern–Volmer quenching constant and $[Q]$ is the concentration of the quencher. Both the F_0 and K_{SV} were the fitted parameters. Notably, attempts to use more complicated models (e.g. two populations of fluorophors with

different quencher accessibility) did not improve the quality of the fit. Therefore, we used the formula given above.

Quenching experiments were performed in four different setups i.e. without any ligand, with 15 mM $MgCl_2$ (Lach-Ner), 15 mM Na_2ATP (Sigma) or 15 mM MgATP (Sigma). The experiments in the absence of magnesium (i.e. free C45, or in the presence of Na_2ATP) were carried out in the presence of 5 mM EDTA. In order to identify the influence of individual ligand on the C45 conformation, quenching constants from at least three independent measurements were compared to the ligand-free experiments quenching constants.

2.4. Time-resolved fluorescence measurements

Time-resolved fluorescence data were obtained by the time-correlated single photon counting (TCSPC) method on the spectrometer PicoHarp 300 (PicoQuant), using the pulsed LED centered at 298 nm (PLS300, PicoQuant) with the pulse frequency 10 MHz and emission monochromator set to 350 nm. Detected photons were collected into a histogram covering the time scale of 100 ns and with a 32 ps/channel resolution. All the experiments were carried out at 20 °C (bath controlled). In the experiments for fluorescence lifetime determination, data were sampled for 20 min under the magic-angle conditions, and 2000–11000 counts in the leading channel were collected in the histogram. In the anisotropy decay experiments with W385 mutant, each I_{VV} and I_{VH} were collected for 10 min and about 8000 counts in the leading channel for I_{VV} was obtained. The G-factor was determined in the separate experiment. The instrument–response function was estimated using the colloid–silica (Ludox) as a scatterer. Fluorescence decays were fitted using the FluoFit 4.2.1 software (PicoQuant) as a sum of exponentials:

$$I(t) = \sum_i \alpha_i \cdot e^{-t/\tau_i}.$$

The intensity-weighted mean fluorescence lifetime was calculated as

$$\tau_M = \frac{\sum \alpha_i \tau_i^2}{\sum \alpha_i \tau_i}.$$

Fluorescence anisotropy decays were fitted by the Pulse5Q software using the maximum entropy method (MEDC, Ltd.). Fluorescence anisotropy decays were analyzed as a sum of exponentials:

$$r(t) = \sum_i \beta_i \cdot e^{-t/\phi_i}$$

where the set of the amplitudes β_i represents a distribution of the correlation times ϕ_i. The β_i are related to the initial anisotropy r_0 by the formula:

$$\sum_i \beta_i = r_0.$$

100 correlation times ϕ_i equidistantly spaced at the logarithmic scale ranging from 50 ps to 100 ns were used.

2.4.1. Molecular modeling

At the beginning of the study, no experimentally determined structure of the entire Na^+/K^+-ATPase C45 was known. Therefore we created the C45 model in the closed conformation (see also Discussion) based on the homology with SERCA and it was used as a starting structure in the molecular dynamic simulations described below. However, during the preparation of the manuscript, the crystal structure of the Na^+/K^+-ATPase at 3.5 Å resolution has been published revealing the open C45 conformation. In order to check the validity of our simulations, we excised the C45 from the crystal structure and the subsequent molecular dynamic simulation revealed that the loop relaxed into the closed conformation, thus, justifying our homology model based molecular dynamic simulations (see below).

2.4.2. Homology model construction

The homology model of the C45 of the Na^+/K^+-ATPase was created using the MOE [29] software package. The C45 sequence was aligned to the sequence of the rabbit SERCA1a and the alignment was manually refined with respect to the known Na^+/K^+-ATPase structural data, namely to the NMR-solved N-domain structure[26] (Suppl. Mat., Fig. S1). Our previous data suggested that the isolated C45 adopted the E2-like conformation; therefore the model was built using the high-resolution structure of SERCA in E2-conformation (PDB entry 2C8L) as a template. Using the default settings and the force-field of the *parm99* [30,31], 10 structures were generated using the fine minimization and the average structure was taken as the initial state for the molecular dynamics simulations. The C-terminal loop of the C45 homology model was truncated by 13 residues in order to reduce computational demands.

2.4.3. Molecular dynamics simulations

Molecular dynamics (MD) simulations have been performed with a homology model of the C45 with sodium or magnesium counterions in the absence of ATP (hereafter C45-Na and C45-Mg), as well as with ATP bound to the active site of C45 (hereafter C45-Na_2ATP and C45-MgATP). The ligand was immersed to the previously relaxed structure of C45-Na using the 1MO8 structure [26] as a template. The ATP phosphates were oriented toward the phosphorylation site of P-domain at D369 residue. The relaxed structure was taken at the time of ~2000 ps from the C45-Na MD simulation. To compensate the negative charge of C45-Na_2ATP and C45-MgATP, 22 Na^+ or 11 Mg^{2+} counterions were added, respectively. To check the quality of C45 homology model simulations, a control MD run at 10 ns time scale with the crystal structure of the Na^+/K^+ ATPase (PDB ID 3B8E[18]) was performed. The MD simulation of unliganded Na^+/K^+ ATPase (denoted as C45-Xray) was carried out with Na^+ counterions to neutralize the system. All simulations were carried out using the SANDER module of AMBER 9.0 [32] suite of programs with the *parm99* force field. The simulation protocol was used as follows: at first all protonation states of histidine residues were checked by visual inspection to maximize H-bond contacts. Then, all hydrogens and individual counterions were added using LEaP program of AMBER 9.0 package. Each system was immersed in a rectangular water box with a minimum distance between the molecule and the box wall of 9 Å. Then, each system was minimized prior to the production part of the molecular dynamics run in the following way. The protein was constrained and the solvent molecules with counterions were allowed to move during a 1000 step minimization followed by 10 ps long molecular dynamics run under [*NpT*] conditions ($p = 1$ atm, $T = 298.15$ K). The next step covers relaxation of side chains by several consequent minimizations with decreasing force constants applied to the backbone atoms. After the relaxation, the entire system was heated. The thermalization protocol was set up as follows: each system was heated from 10 K to 50 K for 20 ps, then from 50 K to 250 K for 20 ps and then from 250 K to 298.15 K for 30 ps. The particle-mesh Ewald (PME) methods for treating electrostatic interactions were used. All simulations were performed under periodic boundary conditions in the [*NpT*] ensemble at 298.15 K and 1 atm using the 2 fs integration step. The SHAKE algorithm with a tolerance of 10^{-5} Å was used to fix positions of all hydrogens. The cutoff of 9.0 Å was applied to treat nonbonding interactions. Coordinates were stored every picosecond. The total duration of the production phases for C45-Na, C45-Mg, C45-Na_2ATP and C45-MgATP is equal to 7 ns, 3.5 ns, 4 ns and 4.5 ns, respectively. The C45-Na system contained in total 60219 atoms (411 residues, 18 Na^+ counterions and 17992 water molecules). The C45-Mg system contained 58983 atoms (411 residues, 9 Mg^{2+} atoms and 17583 water molecules). The C45-Na_2ATP system contained 57431 atoms (411 residues, 22 Na^+ counterions, one ATP molecule and 17047 water molecules). The C45-MgATP contained 57315 atoms (411 residues, 11 Mg^{2+} counterions, one ATP molecule and 17012 water molecules). The C45-Xray

structure contained 52710 atoms (411 residues, 18 Na^+ counterions and 15489 water molecules). The trajectory stability was checked by the root-mean-square-deviation (RMSD) of backbone atoms from the initial structure and radius of gyration (R_g). The RMSD, R_g and secondary structure analysis were calculated by PTRAJ module of AMBER 9.0 package. The radial distribution function (RDF), describes how the density of surrounding matter varies as a function of the distance from a distinguished point. The RDF values of water molecules oxygens at 1.0 nm distance to center of mass of selected residues have been used to assess a spatial accessibility of the residues from solvent.

3. Results

3.1. Expression and purification of the single-tryptophan C45 mutants

The native C45 sequence contains two tryptophanyl residues (W385 and W411). They were subsequently replaced by phenylalanines to obtain a tryptophanless (TL) construct. Further, artificial reporter tryptophans were inserted into this TL construct to yield a set of single-tryptophan mutants. Based on the homology model of the C45 (see below), these reporter tryptophans were placed on the various positions on the C45 surface (Fig. 1). Wherever it was possible, we attempted to perform conserved mutations (i.e. the residue to be replaced by Trp was chosen as aromatic or hydrophobic one), in order to minimize the effect of the mutation on the protein folding. Indeed, expression of all mutants resulted in a high yield of soluble protein (typically >5 mg of purified protein from 0.2 L of the culture), suggesting that the protein tertiary structure was not substantially altered. The purification of the $(His)_6$-tagged protein on the Co^{2+}-affinity column yielded a single band on the SDS-electrophoresis gel (not shown).

3.2. Fluorescence decays

Time-correlated single photon counting (TCSPC) method was used to characterize fluorescence decays of the single-tryptophan mutants at various conditions (without any ligand, in the presence of Mg^{2+}, MgATP or Na_2ATP). All the decays were satisfactorily fitted to the three-exponential decay scheme (Suppl. Mat., Table S1) with reduced χ^2 approaching 1.00, random distribution of the first residuals and the autocorrelation function in all cases (not shown). The only exceptions were all decays of the TL-S732W mutant, decays for TL-V648W mutant in the absence of any ligand and in the presence of Mg^{2+}, which were satisfactorily described by the 2-exponential decay model. The main goal of these experiments was to estimate the mean excited-state lifetime (the penultimate column of the Table S1 in Suppl. Mat.) that characterizes the time, during which the acrylamide can effectively quench the fluorescence.

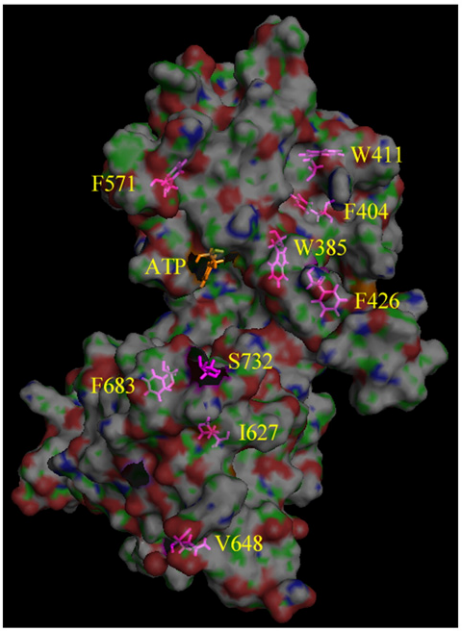

Fig. 1. Reporter positions on the C45. The homology C45 model is displayed with the Connolly type semitransparent surface, the residues that where mutated to the reporter tryptophanyl residue and subsequently evaluated in the spectroscopic experiments are in the stick representation and colored purple.

Table 1

Protein	Location	No substrate	Mg^{2+}	MgATP	Na_2ATP
WT-W411F	N-domain	0.86 ± 0.02	0.78 ± 0.06	0.65 ± 0.02	0.68 ± 0.03
TL-F404W	N-domain	1.79 ± 0.23	1.37 ± 0.17	1.30 ± 0.33	0.98 ± 0.17
WT-W385F	N-domain	1.16 ± 0.08	1.21 ± 0.19	1.13 ± 0.22	1.14 ± 0.22
TL-F426W	N-domain	1.66 ± 0.03	1.46 ± 0.09	1.53 ± 0.09	1.48 ± 0.12
TL-F571W	N-domain	1.77 ± 0.18	1.00 ± 0.12	1.34 ± 0.09	1.28 ± 0.08
TL-I627W	P-domain	0.97 ± 0.07	1.07 ± 0.07	1.05 ± 0.22	0.89 ± 0.18
TL-V648W	P-domain	1.42 ± 0.33	1.36 ± 0.26	1.37 ± 0.19	1.34 ± 0.23
TL-F683W	P-domain	1.33 ± 0.08	1.39 ± 0.26	1.18 ± 0.11	0.92 ± 0.07
TL-S732W	P-domain	1.36 ± 0.07	1.26 ± 0.02	1.25 ± 0.17	1.22 ± 0.09

Bimolecular quenching constants for quenching of the Trp fluorescence by acrylamide given in 10^9 M^{-1} s^{-1} are calculated as the ratio of the Stern–Volmer quenching constants given in Table S2, and the corresponding mean fluorescence lifetime in Table S1. The native sequence of C45 contains two Trp residues on the positions 385 and 411. Thus, WT-W411F or WT-W385F designates mutants where only Trp385 or Trp411 was present, respectively, the other Trp residue was mutated to Phe. For all the other mutants, both the Trp385 and Trp411 were mutated to phenylalanines, and the designation of the protein indicates the position of the reporter Trp residue that was inserted into the tryptophanless mutant.

3.3. Fluorescence quenching by acrylamide

Fluorescence quenching experiments give a unique opportunity to monitor changes of the protein shape. The Stern–Volmer quenching constant (K_{SV}) reflects the effectivity of the quenching (Suppl. Mat., Table S2) and is dependent mainly on the spatial accessibility of the fluorophore and its mean excited-state lifetime (τ_M, Table S1, Suppl. Mat.). Dividing the K_{SV} by τ_M yields the bimolecular quenching constant (k_q, Table 1), which already characterizes the spatial accessibility of the fluorophor. Therefore, even in the experiments without any ligand the k_q varied between 1.79×10^9 M^{-1} s^{-1} for the best accessible tryptophan in the TL-F404W mutant, down to 0.86×10^9 M^{-1} s^{-1} for the worst accessible native W385 residue (WT-W411F mutant), within our set of single-tryptophan mutants (Table 1). Notably, after binding of ligand (Mg^{2+}, MgATP or Na_2ATP) we observed significant k_q changes for the quenching of some tryptophans, as discussed below.

3.4. Mg^{2+} binding

It was expected that binding of this small ligand would induce only subtle changes in the C45 shape that will be hardly detectable. Indeed, quenching of most tryptophans deviated only within the experimental error from the experiments performed in the absence of any ligand. The only exception was the quenching of the TL-F571W mutant (this residue is located on the N-domain), where we observed almost 2-fold decrease in the k_q (from 1.77×10^9 to 1.00×10^9 M^{-1} s^{-1}), reflecting substantial protection of this residue against quenching ($p<0.01$). Notably, the k_q value significantly differs also from the value obtained in the MgATP presence ($p<0.03$, see below), suggesting that the observed effect is a result of free Mg^{2+} binding.

3.5. MgATP binding

We expected that binding of ATP in the presence of magnesium would induce substantial changes in the C45 conformation.

Table 2

Ligand	β_1	β_2	Φ_1 (ns)	Φ_2 (ns)	χ_R^2
None	0.062	0.145	0.053	39.8	1.09
Mg^{2+}	0.060	0.144	0.069	41.5	1.07
MgATP	0.038	0.143	0.069	39.6	1.01
Na_2ATP	0.039	0.133	0.104	31.5	1.05

Anisotropy decay parameters for the native W385 residuum (WT-W411F mutant), β_i are the fractional anisotropies, Φ_i are the corresponding rotational correlation times, reduced χ^2 reflects the goodness of fit.

Surprisingly, the observed changes differed only very slightly from the experiments performed with Mg^{2+} only. Again, quenching of most Trp residues deviated only within the range of experimental error, when compared to the experiments in the absence of any ligand, and the only mutant exhibiting substantial changes was the TL-F571W mutant where we observed decrease in k_q from 1.77×10^9 M^{-1} s^{-1} to 1.34×10^9 M^{-1} s^{-1} ($p<0.06$). This value was significantly different also from that obtained in the presence of Mg^{2+} only ($p<0.03$), but not from that obtained in the Na_2ATP presence ($p<0.51$, see below), suggesting that it is an effect of the ATP binding to nucleotide-binding site on the N-domain. Further, for the native W385 residue (WT-W411F mutant), we observed decrease in k_q from 0.86×10^9 to 0.65×10^9 M^{-1} s^{-1} ($p<0.01$). However, this value does significantly differ neither from that obtained in the Mg^{2+} presence ($p<0.70$) nor in the Na_2ATP presence ($p<0.95$, see below), and it seems that this half-buried native tryptophan is sensitive to binding of all ligands.

3.6. Na_2ATP binding

The most complex changes were observed when the C45 mutants were incubated with the Na_2ATP. The k_q decreased significantly (when compared to the quenching in the absence of any ligand) in the quenching of the native W385 residue (WT-W411F mutant) from 0.86×10^9 to 0.68×10^9 M^{-1} s^{-1} ($p<0.01$), for the TL-F404W mutant from 1.79×10^9 to 0.98×10^9 M^{-1} s^{-1} ($p<0.02$), for the TL-F571W mutant from 1.77×10^9 to 1.28×10^9 M^{-1} s^{-1} ($p<0.05$) and for the TL-F683W mutant from 1.33×10^9 to 0.92×10^9 M^{-1} s^{-1} ($p<0.01$), revealing that also these residues are partially protected against quenching in the Na_2ATP presence. Notably, the changes concerning the N-domain residues (i.e. WT-W411F, TL-F404W and TL-F571W mutants) go in the same direction as in the MgATP presence (mutual comparison of results in the MgATP or Na_2ATP presence yields values of $p<0.38$, $p<0.31$ or $p<0.51$, respectively), but are much more distinct. However, for the TL-F683W mutant, the result significantly differs also in the comparison to the MgATP ($p<0.06$). The quenching of the Trp residues on the other mutants did not significantly differ from the experiments in the absence of any ligand.

3.7. Anisotropy decay

Fluorescence anisotropy contains the information about the mobility of the fluorophor. Typically, time-resolved measurement of the anisotropy decay enables to distinguish three components for the tryptophanyl residue on the protein. The shortest rotation correlation time (typically about 70 ps) corresponds to the movement of Trp side-chain. The middle one (typically in ns time-range) reflects segmental motion, while the longest one reflects rotation of the whole protein, and is therefore dependent on its size (typically tens of ns) [33].

We selected the mutant containing the native W385 residue (WT-W411F mutant) located on the N-domain for the anisotropy decay experiments because according to our model this residue is half-buried, and we expected that it should not exhibit the segmental motion, which simplifies the data analysis. Indeed, the anisotropy decay could be described as a sum of two components (Table 2) in all cases. The ~70 ps correlation time fits well to the values expected for the Trp side-chain movement, and the ~40 ns correlation time observed for the protein without any ligand, in the presence of Mg^{2+} or MgATP could be also expected for the 48 kDa protein. Interestingly, in the presence of ATP alone, this longer component has been shortened to ~30 ns only, reflecting that the N-domain is only weakly linked to the P-domain in this case. In principle, we should observe three components in the anisotropy decay in this situation. As the N-domain constitutes roughly one half of the C45, the longer correlation time should be split to the ~20 ns component reflecting the N-domain "segmental" movement and the ~40 ns component characterizing the C45 rotation. However, resolution the two correlation times differing only by the factor of 2 in this complex system (3-exponential fluorescence decay and 3-exponential anisotropy decay) is beyond the limits of this method, and in fact, we observe only some average value. Note that we cannot safely interpret the increase of the correlation time in the shorter component of the anisotropy decay in the presence of the ATP, as this component is poorly resolved in the experimental setup with 32 ps/channel resolution (we can just detect that it is present).

3.8. Molecular dynamics simulations

3.8.1. The stability of studied systems

All trajectories are stable during the production part of the MD simulations and reliable for further analyses. The trajectory stability confirms RMSD of backbone atoms from the initial structure, R_g and secondary structure analysis. The curve of RMSD against time calculated for the C45-Na system reaches its plateau at ~1.5 ns. The RMSD of C45-Mg system points out that the system equilibrates at ~1 ns. The C45-Na_2ATP system equilibrates within 2 ns and the C45-MgATP system within 1 ns. The time evolution of RMSD of the C45-Xray reaches its plateau at ~2 ns. The R_g values of C45-Na, C45-Mg and C45-MgATP systems fluctuate around the mean values of 24.9 Å, 25.0 Å and 24.9 Å, respectively. However, the R_g of C45-Na_2ATP starts to increase from 25.1 Å after 2 ns reaching a new plateau ($R_g = 25.7$ Å) at ~2.4 ns (Fig. 2). The visual inspection of the C45-Na_2ATP MD simulation unravels that the increase of R_g correlates with opening of both domains (Fig. 3). The domain opening motion can be described by the angle among the N-domain center of mass, center of mass of loops connecting both domains and P-domain center of mass (hereafter angle-m-m-m). The mean value ± SEM of angle-m-m-m calculated from the last nanosecond of C45-Na_2ATP simulation is equal to 129.9° ± 2.1° and is significantly larger than the mean value 121.6° ± 2.9° from the first nanosecond. The angle 129.9° between both domains (C45-Na_2ATP) is also significantly larger than the same angle 117.5° ± 2.1° calculated for C45-MgATP system.

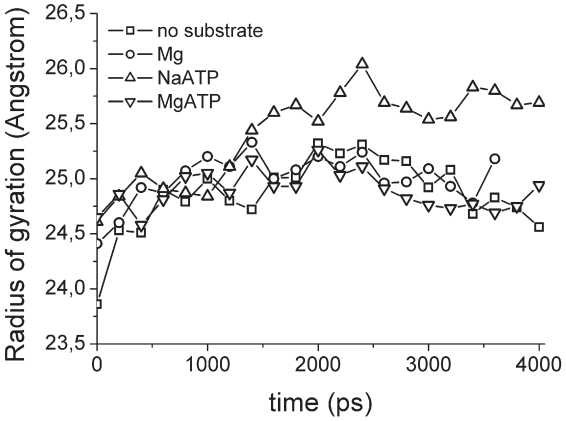

Fig. 2. Overall C45 shape in the MD simulation was evaluated using the radius of gyration. Although this parameter was evaluated every 1 ps of the MD simulation, only the values after every 200 ps are displayed in this graph for clarity. The C45 conformation in the Na_2ATP presence clearly differed from the conformations seen in all the other simulations.

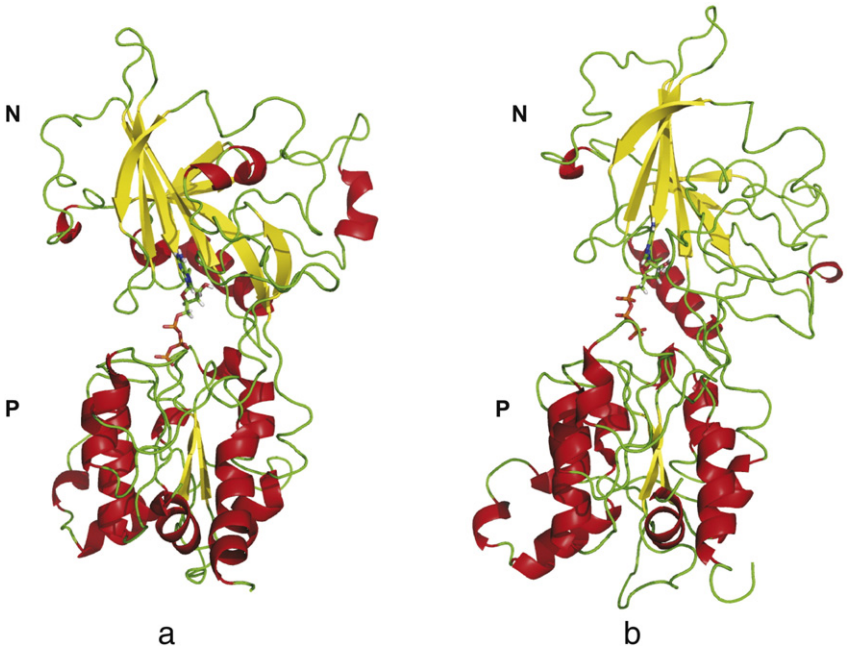

Fig. 3. Two snapshots taken from MD simulation of C45-Na_2ATP system at the beginning and at the end. On the left-hand side there is the equilibrated system of C45-Na_2ATP (700 ps). The angle-m-m-m between N- and P-domains is equal to 117.5°. The figure on the right-hand side shows the snapshot taken from 2250 ps of the corresponding MD simulation. The inter-domain angle is equal to 133.4° and documents opening of both domains.

3.8.2. Structure, dynamics and ATP binding

Generally, the systems containing magnesium ions are less flexible than the systems with sodium ions. The secondary structure is well preserved during all simulations and the highly flexible regions correspond to the loops between secondary structure elements. The N-terminal loop (residues 386–412) is the most flexible segment in all investigated systems. Another flexible C45 loop is formed by residues 422–467. Two loops (residues 625–667 and 721–733) are the most flexible regions of the P-domain.

The ATP molecule is housed by a narrow active site formed by antiparallel β-sheet (residues 481–487 and 496–502), loop of residues 474–480 and loop of residues 540–545 in our models. The ATP purine ring stacks to the F475 benzene ring and ATP N^6H_2 group may form H-bond to D443. The ATP ribose moiety (O2′ and O3′) makes two H-bonds to R544 and D612, respectively. A salt bridge among the α- and β-phosphate moieties and K480 also occurs during simulations. These structural characteristics correspond well to previously published spectroscopic experiments [21–23,26,34].

Two Mg^{2+} counterions are coordinated to α-, β- and γ-phosphates of ATP in the C45-MgATP system, similarly as revealed in SERCA crystallographic studies [16]. One Mg^{2+} ion is housed among D369, V609 backbone oxygen and the ATP γ-phosphate moiety. The other one Mg^{2+} ion resides between ATP α- and β-phosphate group oxygens. Both Mg^{2+} counterions remain in their positions and maintain all abovementioned interactions during the entire MD simulation.

On the other hand, three sodium counterions are tightly bound to ATP phosphate moiety in the C45-Na_2ATP system. In the closed state at the beginning of the simulation, one sodium ion mediates the interaction between D369 and ATP γ-phosphate moiety. As soon as both domains open (interdomain angle increases by ~20°), the interaction between D369 and ATP disrupts. In the open state, two sodium ions mediate the interaction of D612 to ATP β- and γ-phosphates. We assume that the loss of the D369 interaction to ATP starts the domain opening (*cf.* Fig. 3).

3.8.3. Correlation with experimental data

Our homology model corresponds well to the known experimentally determined structural data. Comparison of the C_α's positions of the NMR-solved N-domain and the corresponding part of our C45 yielded RMSD = 1.7 Å, and comparison of the entire C45 structure to the corresponding part of the SERCA (2c8l) yielded RMSD = 1.6 Å. Both these values are lower than a resolution of any available crystallographic data on P-type ATPases. The overall fold and secondary structure elements of the C45 homology model are consistent with the Na^+/K^+ ATPase crystal structure (at 3.5 Å resolution), which has been published during preparation of this manuscript [18]. The crystal structure represents the C45 in the open conformation while the homology model is in the closed state. This fact prevents a direct comparison of entire structures of both systems. To compare both structures we have superimposed N- and P-domains separately (Suppl. Mat. Fig. S2). There was a good agreement in the overall fold for each domain, larger differences were observed only for the loops that were flexible during our molecular dynamic simulations. The active site of the relaxed homology model (after 2 ns MD

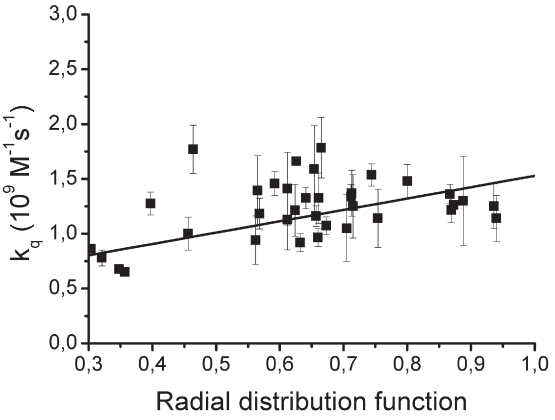

Fig. 4. Correlation between the spectroscopic and modeling data. The accessibility of individual residues in the models was evaluated using the radial distribution function for the 1.0 nm radius around the center of mass of the monitored residues. These values could be directly compared to the bimolecular quenching constants from the acrylamide-quenching experiments. See also text for detailed comments.

simulation of C45-Na) well preserves all main structural features of the active site revealed by the crystal structure (Suppl. Mat. Fig. S3). Only small changes in the side-chains conformations occur for residues Arg544 and Asp443 and can be explained by the flexibility of these residues. Hence, we can conclude that the homology model saves main structural and functional features of the C45 system.

Notably, there is also a good correlation ($p<0.0001$) between spectroscopic and modeling experiments (Fig. 4). The solvent accessibility of a residue in the model could be evaluated by RDF that estimates number of water molecules within the sphere of given radius. The value could be directly compared to the Stern–Volmer quenching constant from the acrylamide-quenching experiments, which is also proportional to the steric angle around the residue accessible from the solvent. Further, the anisotropy decay experiments performed in this study (Table 2) reflected a weak linking of the N- and P-domains in the case of the C45-Na_2ATP system while a tighter one in the case of C45-MgATP system. This fact well coincides with the number of H-bonds between both domains calculated as a mean from the last 2 ns of MD simulations. The numbers of interdomain H-bonds are equal to 4.0 ± 1.9 and 9.5 ± 2.3 for the C45-Na_2ATP and C45-MgATP, respectively, where ATP is considered as an integral part of the N-domain. The introduced terminology "open" and "closed" conformation of the enzyme is attributed the state of the cytoplasmic headpiece. In the open conformation, the N-domain is loosely connected to the other cytoplasmic domains, while in the closed conformation it is closely connected to the P- and A-domains and displays multiple interdomain hydrogen bonds. In this sense, we use the terminology analogously, despite the A-domain is missing in our case.

4. Discussion

Several crystallographic structures of SERCA in various conformations were published [7–16], and recently, also the first crystal structure of Na^+/K^+-ATPase appeared [18]. There are numerous

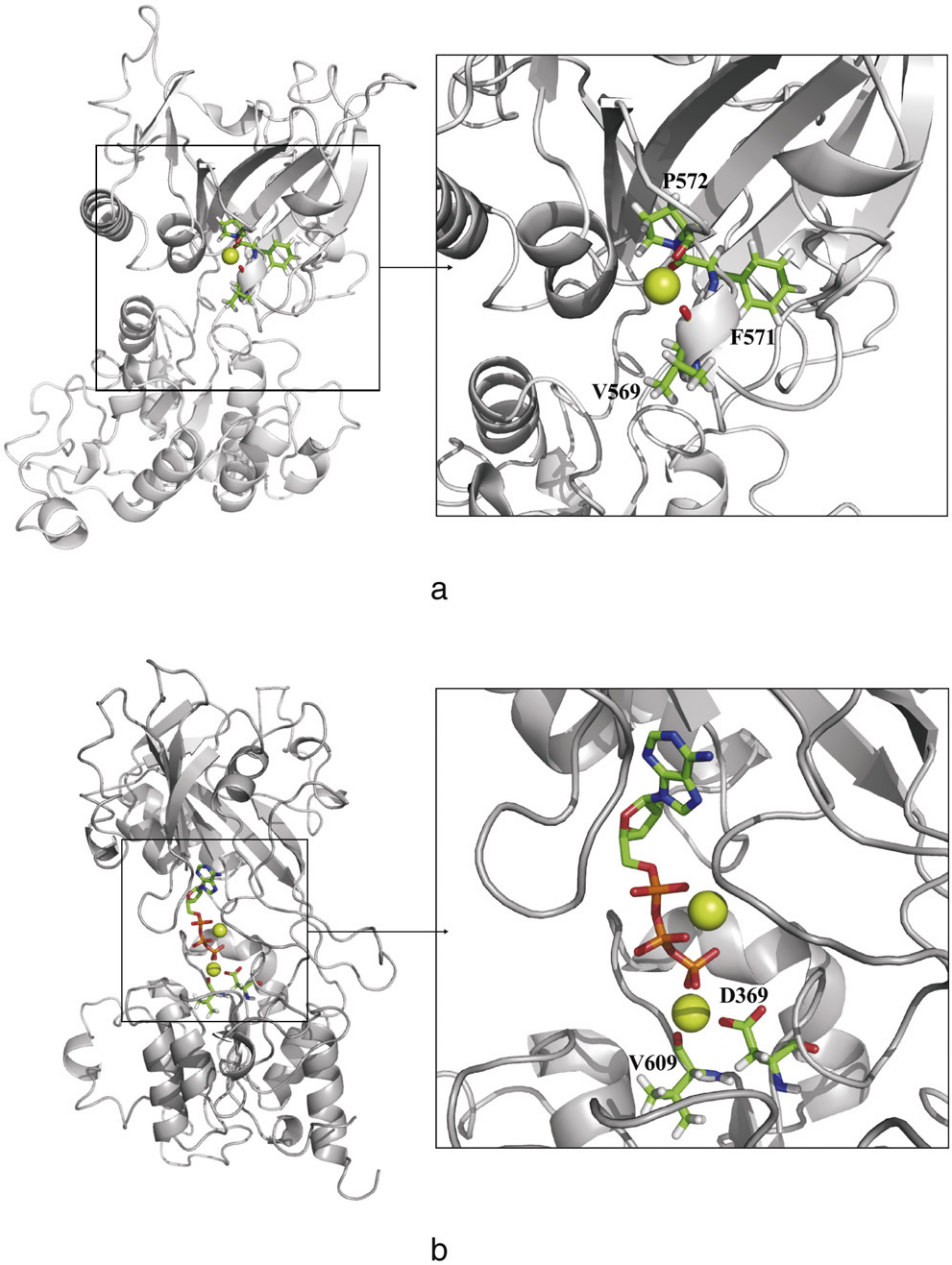

Fig. 5. Mg^{2+}-binding sites. (a) Coordination of the Mg^{2+} in the proximity of Phe571. (b) Coordination of the Mg^{2+} in the proximity of the triphosphate chain. ATP and residues coordinating Mg^{2+} cations are depicted in stick representation, magnesium cations are depicted as green spheres. In the left-hand side pictures, N-domain is on the top.

indications that SERCA is a good representative of all P-type ATPases (or at least Type II ones) and that the displayed conformations are highly relevant also for Na^+/K^+-ATPase [17,35]. Nevertheless, the crystallographic approach has some substantial drawbacks, as thoroughly discussed in [35]. First, it provides only static picture. Moreover, spectroscopic experiments performed under physiological conditions revealed that the protein crystals obtained under very extreme conditions can inevitably influence substantial details in the resolved structure [36]. Finally, all the crystallographic structures displayed enzymes complexed only with molecules that are incompatible with enzyme function, e.g. nucleotide analogs functioning as inhibitors. Thus, in order to observe the protein dynamics under physiological conditions and with native ligands, the conventional spectroscopic techniques and molecular dynamic simulations are the preferred methods of choice [37]. Notably, experimental monitoring of the fine dynamics of the entire transmembrane enzyme encounters serious practical difficulties and presents still a challenge for the future work. Fortunately, the isolated C45 retains the same structural and dynamic features as when being a part of the entire enzyme, and represents a useful system for the studies of the enzyme dynamics, as discussed below.

Our previous results indicated that the isolated C45 contains the low-affinity ATP-binding site [21–25], and similar results were reported also from other laboratories for the isolated C45 of various P-type superfamily members [19,20,38,39]. Moreover, the NMR studies revealed that the structure of the isolated N-domain in the absence of any substrate fits better to the N-domain of SERCA crystallized in the E2 conformation [26]. This corresponds well also to our observations in the molecular dynamic experiments. The C45 homology model turned out to be stable during subsequent molecular dynamic simulation only when it was built on the basis of the 2C8L (E2 conformation) template, in contrast to the model based on the 1SU4 template (E1 conformation, not shown). The recently published Na^+/K^+-ATPase crystal structure revealed the state with the open conformation of C45. Nevertheless, when we excised the C45 from this structure, it rapidly relaxed into the closed conformation during the C45-Xray MD simulation (data not shown). Thus, we can conclude that isolated C45 adopts in the absence of any substrate the closed conformation characteristic for the E2 state.

It was expected that Mg^{2+} itself could hardly dramatically influence the C45 structure. Indeed, most observed experimental parameters varied only slightly and also molecular dynamic simulation revealed that the C45 remained in the closed conformation with one Mg^{2+} cation coordinated by residues D369 and D710 that were already identified in previous studies [40]. Experimental data revealed changes in the environment of the F571 and the molecular model suggested that it may be a consequence of the coordination of one Mg^{2+} cation by the main-chain oxygens of V569 and P572 (Fig. 5a). It should be noted that this site is rather distal to all known important binding sites on Na^+/K^+-ATPase, and thus, it is not clear whether this second Mg^{2+}-binding site could have any physiological importance.

Also in the case when ATP was bound to the C45 in the presence of magnesium, the changes in the C45 conformation were rather small and it preserved the closed conformation. It could be concluded that the MgATP stabilized the closed conformation of the C45. Notably, there were two magnesium cations coordinated by the nucleotide triphosphate chain, similarly as revealed in the crystal structures of SERCA [16]. One of the cations was coordinated by the oxygens of the α- and β-phosphates, the other one was positioned between the γ-phosphate and phosphorylation site at D369, with the assistance of the main-chain oxygen of V609 (Fig. 5b).

The most dramatic changes in all measured parameters were observed in both the spectroscopic experiments and molecular dynamic simulations when ATP was bound to the C45 in the absence of magnesium (Na_2ATP). The fluorescence anisotropy decay experiments revealed that the contact between N- and P-domains was weakened after Na_2ATP binding, which is in good agreement with our molecular dynamic simulations, where we observed rapid opening of the C45, resembling the open conformation observed for the SERCA crystal in the E1-2Ca conformation [7]. Obviously, the huge global conformational change was reflected also by the local changes within various C45 parts. This was reflected also in our spectroscopic experiments, where numerous residues on both the N- and P-domains exhibited changes in its accessibility (see Results).

4.1. Usability and limits of the isolated C45

The obvious question arises, how much are the experiments with the isolated C45 relevant also for the entire enzyme. As discussed above, the isolated C45 seems to support its tertiary structure, and our data suggest that the C45 can adopt the open and close conformations, i.e. dynamic behavior expected for this loop when being part of the entire enzyme. Finally, it is necessary to analyze some logical consequences to the Albers–Post cycle, which is usually used for description of the P-type ATPases working mechanism. It postulates that the enzyme adopts two major conformations during the catalytic cycle. One of them, traditionally designated as E1, has high affinity to both ATP and sodium and low affinity to potassium ions. Contrary, the E2 conformation has low affinity to both ATP and sodium and high affinity to potassium ions. Already early experiments of Skou revealed that magnesium must be present in the cytoplasm as an essential cofactor that is not transported to the other side of the membrane. The fact that recent experiments located the Mg^{2+}-binding site in the proximity of the phosphorylation site lead to the consideration of MgATP as the only true P-type ATPases ligand [41,42] and it is generally agreed that magnesium is essential for the phosphorylation of the conserved aspartyl residue (D369 on Na^+/K^+-ATPase). Additionally, it is known that ATP can bind also to the enzyme in the E2 conformation, although with lower affinity (K_M ~ 200 μM).

As discussed above, the isolated C45 without any substrate adopts the closed conformation that was attributed to the E2 state. Our experiments and molecular dynamic simulation revealed that binding of Mg^{2+} or MgATP does not substantially alter the C45 conformation. In contrast, binding of the Na_2ATP resulted in the rapid mutual movement of both N- and P-domains yielding the open conformation, which is characteristic for the E1 state. Moreover, subsequent addition of Mg^{2+} induced the C45 closure again (Fig. 6). However, it should be noted that this conformation (after subsequent addition of ATP and Mg) turned out to be unstable in molecular dynamic simulation on longer time scales, and we observed some kind of oscillations.

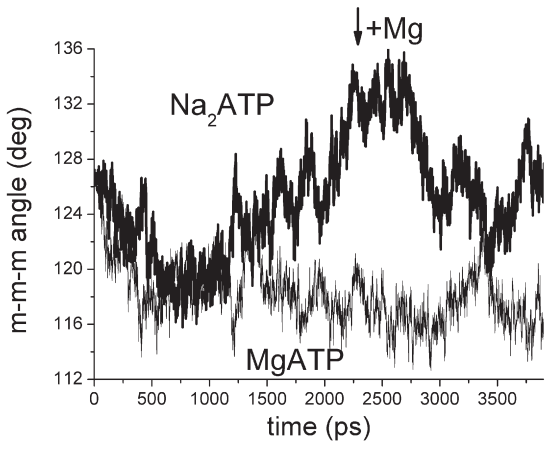

Fig. 6. Opening and closing of the C45. The angle between centers of mass of the N- and P-domain and the hinge between these two domains was monitored during the MD simulations. Addition of the pure ATP the closed C45 conformation induced rapid repulsion of the domains, while subsequent addition of magnesium enabled closure of the domains. Notably, addition of the MgATP left the loop in the closed conformation.

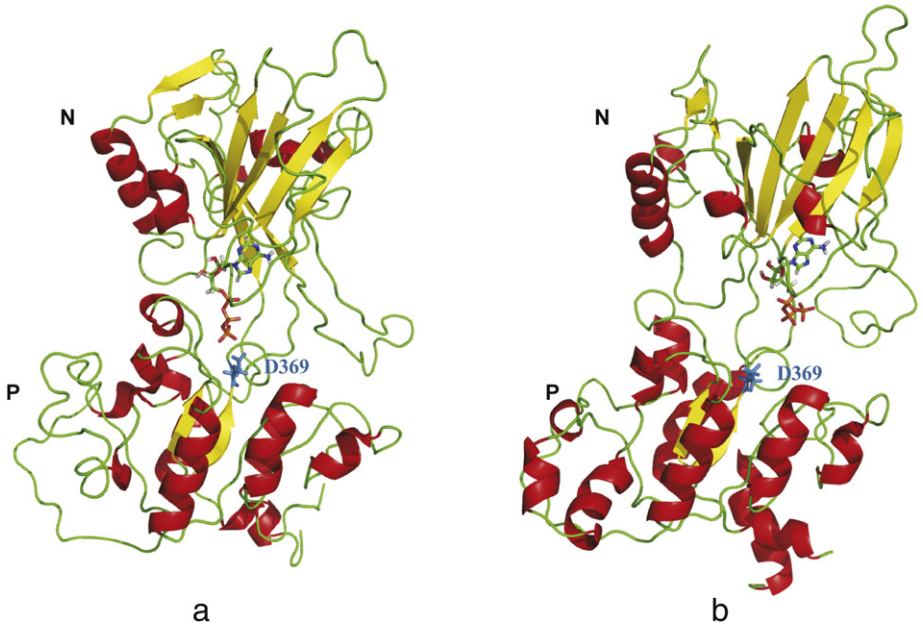

Fig. 7. Comparison of the C45 structures when the MgATP was bound at once and when ATP and Mg^{2+} were bound subsequently (last frames from the experiments described in Fig. 6).

Comparison with the closed conformation where the Mg and ATP were added at once (and which was very stable on the long time scales) revealed that the difference consists in ~20° mutual rotation of the N- and P-domains with respect to the axis perpendicular to the membrane (Fig. 7) and the γ-phosphate cannot properly reach the phosphorylation site, which is in agreement with previous findings that the isolated C45 cannot efficiently hydrolyze the ATP [43]. Apparently, here we encountered the limits of the isolated C45 system. Based on the crystal structures of SERCA, where the A-domain was in the contact with both the N- and P-domains, we suggest that the flanking stroke of the A-domain into C45 is necessary to correct the mutual orientation of the N- and P-domains. Unfortunately, this could not have been observed in our studies with the isolated C45.

Our experiments suggested that the state of the cytoplasmic headpiece may not be related to the binding of the transported cations to the transmembrane domain. It correlates with the observation that the cytoplasmic headpiece in the crystal structures of SERCA obtained in the presence of Ca^{2+} ions can be found in the open (PDB ID: 1SU4) or closed (PDB ID: 1T5S) conformation. Our experiments suggest that C45 conformation depends on the presence or absence of the nucleotide and magnesium; the open conformation is found only for Na_2ATP bound to the C45, in all the other cases (i.e. Mg^{2+}, Mg + ATP or an empty loop) the C45 is closed.

Based on these observations, it seems reasonable to describe the conformation of the cytoplasmic- and transmembrane domains within the Albers-Post cycle independently, and instead of traditional E1 and E2 to use $^{o/c}E_{Na/K}$, where the superscript "o" or "c" denotes the open or closed conformation of the cytoplasmic headpiece, and the subscript "Na" or "K" reflects the high affinity of the sodium or potassium ions to the transmembrane domain (Fig. 8). In contrast to the previously published models, binding of ATP and Mg^{2+} occurs at different steps of the catalytic cycle. ATP binding induces the $^{c}E_{K} \rightarrow {}^{o}E_{K}$ conformational change. This conformational change is transmitted to the transmembrane domain yielding the $^{o}E_{K} \rightarrow {}^{o}E_{Na}$ and the cations can be exchanged on the cytoplasmic side. Only then, binding of the Mg^{2+} causes the $^{o}E_{Na} \rightarrow {}^{c}E_{Na}$ transition, enabling the ATP hydrolysis and the enzyme phosphorylation (notably, the ADP bound form is probably only a transient state). This is the impulse for the $^{c}E_{Na} \rightarrow {}^{c}E_{K}$ transition and the cation exchange on the extracellular side can take place. Potassium binding induces phosphate and Mg^{2+} release and the enzyme is ready to bind another ATP molecule — the cycle is completed. Logically, the alternative conformational changes in the cytoplasmic headpiece (CH) and transmembrane domain (TD), i.e. CH → TD → CH → TD → etc., seem to be an essential feature that supports the vectoriality of the cation transport.

This scheme fits well to the generally known fact that Mg^{2+} is essential for the enzyme phosphorylation. Moreover, it seems to provide the structural explanation for the results of kinetic experiments performed by Plesner and Plesner [44] on the entire enzyme. They demonstrated that the cytoplasmic ligands can bind

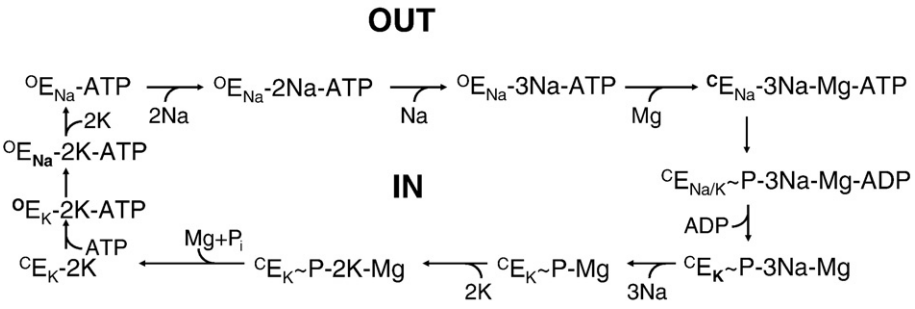

Fig. 8. Proposed modification of the Albers–Post model based on our experiments. See text for detailed comments.

subsequently to the enzyme also in the dissociated form, ATP being bound to the enzyme as the first ligand, and Mg^{2+} as the second one. It should be stressed that the estimated affinity of the ATP to the so-called low-affinity binding site (~200 μM) should be fully sufficient for the proper enzyme work under physiological cytoplasmic free ATP concentrations (~600 μM, assuming 3 mM total ATP concentration, and considering the Mg + ATP ↔ MgATP equilibrium; under cytoplasmic ionic strength, approx. 20% of the nucleotide should be in the free ATP form). In fact, such an affinity enables much finer regulation than eventual modulation of the high-affinity binding site (K_M~0.2 μM). With subtle differences, similar hypothesis was recently proposed by Jensen et al. [13] based on the experiments with SERCA. They postulated that ATP binds in fact to the low-affinity (or modulatory, in Jensen's terminology) site, which is later converted to the high-affinity (or catalytic, in Jensen's terminology) site. Finally, the proposed scheme is also in agreement with experiments, where the conformational change was observed as a consequence of sodium/potassium exchange [45]. They can be attributed to the $^{o}E_K \rightarrow {}^{o}E_{Na}$ or $^{c}E_{Na} \rightarrow {}^{c}E_K$ transitions in our scheme.

5. Conclusion

Series of successful crystallographic experiments on SERCA provided good structural basis for understanding of the P-type ATPases working mechanism. Our experiments examining the dynamics of the enzyme complement these data. The work with the isolated C45 enabled efficient separation of the events occurring within the transmembrane- and cytoplasmic parts of the Na^+/K^+-ATPase during the pumping cycle. Combination of the intrinsic tryptophan fluorescence experiments and molecular dynamics simulation suggested fine coordination of the cytoplasmic ligands (ATP and Mg^{2+}) binding in order to drive the opening and closure of the cytoplasmic domains. Based on our results and in agreement with numerous previously published experiments performed with the entire enzyme, we propose that free ATP is bound to the low-affinity binding site inducing opening of the cytoplasmic headpiece (traditionally denoted as E2 → E1 transition). Magnesium is bound later and induces closure of the cytoplasmic headpiece, thus (likely with the A-domain assistance) enabling autophosphorylation (traditionally denoted as E1 → E2 transition). However, we cannot exclude that the catalytic cycle is more complex, and our mechanism of sequential binding of ATP and Mg^{2+} represents only part of this scheme and that MgATP can be bound in some other part of the catalytic cycle. This possibility could be very attractive namely in models assuming oligomeric cooperation of two or more subunits [46–48]. Obviously, although our conclusions fit well to the recent state of knowledge about the pumping mechanism, it will be necessary to prove our proposals also in the experiments with the entire enzyme, which still presents a challenging task.

Acknowledgements

This work was supported by the grants of the Czech Science Foundation GACR 203/07/0564, GACR 522-08-H003 and GACR 303/07/0915, and the research projects of Czech Ministry of Schools, Youth and Sports LC512, MSM 6198959215 and MSM 6198959216.

Appendix A. Supplementary data

Supplementary data associated with this article can be found, in the online version, at doi:10.1016/j.bbamem.2009.02.004.

References

[1] K.B. Axelsen, M.G. Palmgren, Evolution of substrate specificities in the P-type ATPase superfamily, J. Mol. Evol. 46 (1998) 84–101.
[2] R.W. Albers, Biochemical aspects of active transport, Annu. Rev. Biochem. 36 (1967) 727–756.
[3] R.L. Post, S. Kume, C. Hegyvary, Activation by adenosine-triphosphate in phosphorylation kinetics of sodium and potassium ion transport adenosine-triphosphatase, J. Biol. Chem. 247 (1972) 6530–6540.
[4] J.C. Skou, Further investigations on a Mg++ + Na+-activated adenosintriphosphatase, possibly related to the active, linked transport of Na+ and K+ across the nerve membrane, Biochim. Biophys. Acta 42 (1960) 6–23.
[5] J.V. Moller, B. Juul, M. leMaire, Structural organization, ion transport, and energy transduction of P-type ATPases, Biochim. Biophys. Acta-Rev. Biomembr. 1286 (1996) 1–51.
[6] K. Geering, The functional role of beta subunits in oligomeric P-type ATPases, J. Bioenerg. Biomembranes 33 (2001) 425–438.
[7] C. Toyoshima, M. Nakasako, H. Nomura, H. Ogawa, Crystal structure of the calcium pump of sarcoplasmic reticulum at 2.6 angstrom resolution, Nature 405 (2000) 647–655.
[8] M. Takahashi, Y. Kondou, C. Toyoshima, Interdomain communication in calcium pump as revealed in the crystal structures with transmembrane inhibitors, Proc. Natl. Acad. Sci. U. S. A. 104 (2007) 5800–5805.
[9] K. Obara, N. Miyashita, C. Xu, L. Toyoshima, Y. Sugita, G. Inesi, C. Toyoshima, Structural role of countertransport revealed in Ca2+ pump crystal structure in the absence of Ca2+, Proc. Natl. Acad. Sci. U. S. A. 102 (2005) 14489–14496.
[10] C. Toyoshima, T. Mizutani, Crystal structure of the calcium pump with a bound ATP analogue, Nature 430 (2004) 529–535.
[11] C. Toyoshima, H. Nomura, Structural changes in the calcium pump accompanying the dissociation of calcium, Nature 418 (2002) 605–611.
[12] T.L.M. Sorensen, C. Olesen, A.M.L. Jensen, J.V. Moller, P. Nissen, Crystals of sarcoplasmic reticulum Ca2+-ATPase, J. Biotechnol. 124 (2006) 704–716.
[13] A.M.L. Jensen, T.L.M. Sorensen, C. Olesen, J.V. Moller, P. Nissen, Modulatory and catalytic modes of ATP binding by the calcium pump, EMBO J. 25 (2006) 2305–2314.
[14] J.V. Moller, C. Olesen, A.M.L. Jensen, P. Nissen, The structural basis for coupling of Ca2+ transport to ATP hydrolysis by the sarcoplasmic reticulum Ca2+-ATPase, J. Bioenerg. Biomembranes 37 (2005) 359–364.
[15] C. Olesen, T.L.M. Sorensen, R.C. Nielsen, J.V. Moller, P. Nissen, Dephosphorylation of the calcium pump coupled to counterion occlusion, Science 306 (2004) 2251–2255.
[16] T.L.M. Sorensen, J.V. Moller, P. Nissen, Phosphoryl transfer and calcium ion occlusion in the calcium pump, Science 304 (2004) 1672–1675.
[17] K.J. Sweadner, C. Donnet, Structural similarities of Na,K-ATPase and SERCA, the Ca2+-ATPase of the sarcoplasmic reticulum, Biochem. J. 356 (2001) 685–704.
[18] J.P. Morth, B.P. Pedersen, M.S. Toustrup-Jensen, T.L.M. Sorensen, J. Petersen, J.P. Andersen, B. Vilsen, P. Nissen, Crystal structure of the sodium–potassium pump, Nature 450 (2007) 1043–U1046.
[19] C.M. Tran, R.A. Farley, Catalytic activity of an isolated domain of Na,K-ATPase expressed in *Escherichia coli*, Biophys. J. 77 (1999) 258–266.
[20] C. Gatto, A.X. Wang, J.H. Kaplan, The M4M5 cytoplasmic loop of the Na,K-ATPase, overexpressed in *Escherichia coli*, binds nucleoside triphosphates with the same selectivity as the intact native protein, J. Biol. Chem. 273 (1998) 10578–10585.
[21] M. Kubala, K. Hofbauerova, R. Ettrich, V. Kopecky, R. Krumscheid, J. Plasek, J. Teisinger, W. Schoner, E. Amler, Phe(475) and Glu(446) but not Ser(445) participate in ATP-binding to the alpha-subunit of Na+/K+-ATPase, Biochem. Biophys. Res. Commun. 297 (2002) 154–159.
[22] M. Kubala, J. Teisinger, R. Ettrich, K. Hofbauerova, V. Kopecky, V. Baumruk, R. Krumscheid, J. Plasek, W. Schoner, E. Amler, Eight amino acids form the ATP recognition site of Na+/K+-ATPase, Biochemistry 42 (2003) 6446–6452.
[23] Z. Lansky, M. Kubala, R. Ettrich, M. Kuty, J. Plasek, J. Teisinger, W. Schoner, E.E. Amler, The hydrogen bonds between Arg(423) and Glu(472) and other key residues, Asp(443), Ser(477), and Pro(489), are responsible for the formation and a different positioning of TNP-ATP and ATP within the nucleotide-binding site of Na+/K+-ATPase, Biochemistry 43 (2004) 8303–8311.
[24] M. Kubala, J. Plasek, E. Amler, Limitations in linearized analyses of binding equilibria: binding of TNP-ATP to the H-4-H-5 loop of Na/K-ATPase, Eur. Biophys. J. Biophys. Lett. 32 (2003) 363–369.
[25] M. Kubala, J. Plasek, E. Amler, Fluorescence competition assay for the assessment of ATP binding to an isolated domain of Na+,K+-ATPase, Physiol. Res. 53 (2004) 109–113.
[26] M. Hilge, G. Siegal, G.W. Vuister, P. Guntert, S.M. Gloor, J.P. Abrahams, ATP-induced conformational changes of the nucleotide-binding domain of Na,K-ATPase, Nat. Struct. Biol. 10 (2003) 468–474.
[27] T. Obsil, F. Merola, A. Lewit-Bentley, E. Amler, The isolated H-4–H-5 cytoplasmic loop of Na,K-ATPase overexpressed in *Escherichia coli* retains its ability to bind ATP, FEBS Lett. 426 (1998) 297–300.
[28] M.M. Bradford, Rapid and sensitive method for quantitation of microgram quantities of protein utilizing principle of protein-dye binding, Anal. Biochem. 72 (1976) 248–254.
[29] C.C.G. Inc., Molecular Operating Environment (MOE), Canada, 2006.
[30] W.D. Cornell, P. Cieplak, C.I. Bayly, I.R. Gould, K.M. Merz, D.M. Ferguson, D.C. Spellmeyer, T. Fox, J.W. Caldwell, P.A. Kollman, A 2nd generation force-field for the simulation of proteins, nucleic-acids, and organic-molecules, J. Am. Chem. Soc. 117 (1995) 5179–5197.
[31] J.M. Wang, P. Cieplak, P.A. Kollman, How well does a restrained electrostatic potential (RESP) model perform in calculating conformational energies of organic and biological molecules? J. Comput. Chem. 21 (2000) 1049–1074.
[32] D.A. Pearlman, D.A. Case, J.W. Caldwell, W.S. Ross, T.E. Cheatham, S. Debolt, D. Ferguson, G. Seibel, P. Kollman, AMBER, a package of computer-programs for

applying molecular mechanics, normal-mode analysis, molecular-dynamics and free-energy calculations to simulate the structural and energetic properties of molecules, Comput. Phys. Commun. 91 (1995) 1–41.
[33] J.R. Lakowicz, Principles of Fluorescence Spectroscopy, Kluwer/Plenum, New York, 1999, pp. 496–499.
[34] H.R. Hinz, T.L. Kirley, Lysine-480 is an essential residue in the putative ATP site of lamb kidney (Na,K)-Atpase — identification of the pyridoxal 5′-diphospho-5′-adenosine and pyridoxal-phosphate reactive residue, J. Biol. Chem. 265 (1990) 10260–10265.
[35] M. Kubala, ATP-binding to P-type ATPases as revealed by biochemical, spectroscopic, and crystallographic experiments, Proteins-Struct. Funct. Bioinformatics 64 (2006) 1–12.
[36] M. Picard, C. Toyoshima, P. Champeil, The average conformation at micromolar [Ca2+] of Ca2+-ATPase with bound nucleotide differs from that adopted with the transition state analog ADP center dot AlFx or with AMPPCP under crystallization conditions at millimolar [Ca2+], J. Biol. Chem. 280 (2005) 18745–18754.
[37] M. Kubala, T. Obsil, V. Obsilova, Z. Lansky, E. Amler, Protein modeling combined with spectroscopic techniques: an attractive quick alternative to obtain structural information, Physiol. Res. 53 (2004) S187–S197.
[38] M. Abu-Abed, T.K. Mal, M. Kainosho, D.H. MacLennan, M. Ikura, Characterization of the ATP-binding domain of the sarco(endo)plasmic reticulum Ca2+-ATPase: probing nucleotide binding by multidimensional NMR, Biochemistry 41 (2002) 1156–1164.
[39] E. Capieaux, C. Rapin, D. Thines, Y. Dupont, A. Goffeau, Overexpression in *Escherichia-coli* and purification of an ATP-binding peptide from the yeast plasma-membrane H+-Atpase, J. Biol. Chem. 268 (1993) 21895–21900.
[40] G. Patchornik, R. Goldshleger, S.J.D. Karlish, The complex ATP-Fe2+ serves as a specific affinity cleavage reagent in ATP-Mg2+ sites of a Na,K-ATPase: altered ligation of Fe2+ (Mg2+) ions accompanies the E1P→E2P conformational change, Proc. Natl. Acad. Sci. U. S. A. 97 (2000) 11954–11959.
[41] P.A. Pedersen, J.R. Jorgensen, P.L. Jorgensen, Importance of conserved alpha-subunit segment (709)GDGVND for Mg2+ binding, phosphorylation, and energy transduction in Na,K-ATPase, J. Biol. Chem. 275 (2000) 37588–37595.
[42] J.E. Mahaney, D.D. Thomas, J.P. Froehlich, The time-dependent distribution of phosphorylated intermediates in native sarcoplasmic reticulum Ca2+-ATPase from skeletal muscle is not compatible with a linear kinetic model, Biochemistry 43 (2004) 4400–4416.
[43] R. Krumscheid, K. Suankova, R. Ettrich, J. Teisinger, E. Amler, W. Schoner, Localization of catalytic active sites in the large cytoplasmic domain of Na+/K+-ATPase, Na,K-Atpase and Related Cation Pumps, vol. 986, New York Acad Sciences, New York, 2003, pp. 242–244.
[44] L. Plesner, I.W. Plesner, The steady-state kinetic mechanism of ATP hydrolysis catalyzed by membrane-bound (Na++K+)-ATPase from ox brain. 1. Substrate identity, Biochim. Biophys. Acta 643 (1981) 449–462.
[45] S.J.D. Karlish, D.W. Yates, Tryptophan fluorescence of (Na++K+)-ATPase as a tool for study of enzyme mechanism, Biochim. Biophys. Acta 527 (1978) 115–130.
[46] D. Thoenges, E. Amler, T. Eckert, W. Schoner, Tight binding of bulky fluorescent derivatives of adenosine to the low affinity E(2)ATP site leads to inhibition of Na+/K+-ATPase — Analysis of structural requirements of fluorescent ATP derivatives with a Koshland–Nemethy–Filmer model of two interacting ATP sites, J. Biol. Chem. 274 (1999) 1971–1978.
[47] K. Tanoue, S. Kaya, Y. Hayashi, K. Abe, T. Imagawa, K. Taniguchi, K. Sakaguchil, New evidence for ATP binding induced catalytic subunit interactions in pig kidney Na/K-ATPase, J. Biochem. 140 (2006) 599–607.
[48] R.J. Clarke, D.J. Kane, Two gears of pumping by the sodium pump, Biophys. J. 93 (2007) 4187–4196.